Modelling development of acidification within corroding sites on spent fuel surfaces

Z. Qin*[1], W.-J. Cheong[2], P. G. Keech[3], J. C. Wren[1] and D. W. Shoesmith[1,4]

A model has been developed to predict whether the development of acidity is feasible within actively corroding sites on spent nuclear fuel (UO_2) surfaces inside a failed nuclear waste container. The model simulations demonstrate that the build-up of acidity is possible within flaws and pores in a corroded UO_2 surface, providing the separation of anodes and cathodes occurs. The extent to which the pH can be depressed is determined by the dissolution rate of the fuel, the dimensions of the defect, the local redox conditions which determine the corrosion potential, and the fraction of the fuel surface that is reactive. Based on the anticipated redox conditions established radiolytically in a failed container it is shown that a suppression of the pH sufficient to accelerate dissolution (pH$\leq$5) is very unlikely.

Keywords: Acidity, Nuclear materials, Modelling studies, Diffusion, Hydrolysis

***This paper is part of a special issue on 'Long-Term Prediction of Corrosion Damage in Nuclear Waste Systems'***

Introduction

It has been proposed that Canadian spent nuclear fuel (UO_2) be disposed of in a stable deep geologic repository.[1] The fuel bundles would be sealed in corrosion resistant containers, emplaced in bentonite clay and the repository backfilled with a mixture of crushed rock and clay. Corrosion models predict that minimal damage, insufficient to cause failure, will be incurred.[2] However, it is judicious to analyse the consequences of failure when the spent fuel could be exposed to groundwater, and corrosion of the fuel driven radiolytically.

The oxidation/dissolution of UO_2 proceeds in stages[3–5]

$$UO_2 \rightarrow U^{IV}_{1-2x}U^{V}_{2x}O_{2+x} \rightarrow (U^{VI}O_2^{2+})_{aq} \rightarrow U^{VI}O_3 \cdot yH_2O \tag{1}$$
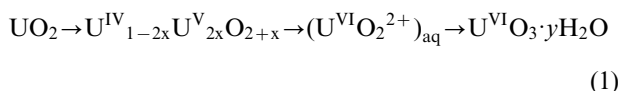
where $U^{VI}O_3.yH_2O$ is a corrosion product that is likely to deposit on the fuel surface. Such deposits would be expected to block corrosion to an extent determined by the porosity of the deposit and to restrict diffusive mass transport of species to and from the reactive fuel surface. However, there is also the possibility of restricted diffusion of dissolved UO_2^{2+} away from the dissolving surface which could react with water to produce hydroxyl-containing U^{VI} species and local acidity near the fuel surface

$$nU^{VI}O_2^{2+} + yH_2O \rightarrow (U^{VI}O_2)_n(OH)_y^{(2n-y)+} + yH^+ \tag{2}$$
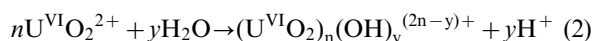
as illustrated in Fig. 1a. This would establish a pH gradient within pores (or flaws in the substrate $U^{IV}O_2$) and, since $U^{VI}O_2^{2+}$ solubility increases as the pH decreases,[6] an inversion of the solubility gradient, leading to transport of $U^{VI}O_2^{2+}$ out of the pores/flaws which would, hence, be maintained open (Fig. 1b).

Such a process has been demonstrated electrochemically[7] when the anode and cathode are separated within the cell. Under corrosion conditions such a separation would not necessarily be achieved and at least partial neutralisation would be expected due to OH$^-$ produced by the cathodic reaction (the reduction of radiolytically produced H_2O_2)

$$H_2O_2 + 2e^- \rightarrow 2OH^- \tag{3}$$
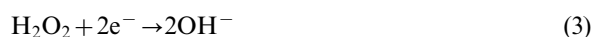
However, corrosion experiments on spent fuel in the presence of dissolved O_2 and high γ/β radiation fields[8] and on unirradiated UO_2 electrodes in close proximity to α-radiation sources[9] showed acidic conditions and the suspected formation of corrosion product deposits. These experiments were conducted at high radiation dose rates. However, within a failed waste container, γ/β fields (after a few hundred years) would be negligible and α-dose rates orders of magnitude lower than those used experimentally.[10,11] This makes meaningful experiments difficult, if not impossible.

Consequently, we have modelled whether or not acidification is possible based on the extrapolation of dissolution rates measured electrochemically. The primary goal of the model is to determine whether acidification within pores in a corrosion product deposit is achievable at the slow rates of fuel corrosion anticipated within a failed waste container.

Model

The model considers anodic dissolution of $U^{IV}O_2$ at the bottom of a pore in a corrosion product deposit, and the development of acidity within the pore due to hydrolysis

[1]Department of Chemistry, The University of Western Ontario, London, Ontario N6A 5B7, Canada
[2]Candu Energy Incorporated, Sheridan Park, Mississauga, Ontario L5B 1K1, Canada
[3]Nuclear Waste Management Organization, Toronto, Ontario M4T 2S3, Canada
[4]Surface Science Western, The University of Western Ontario, London, Ontario N6G 0J3, Canada

*Corresponding author, email zqin@uwo.ca
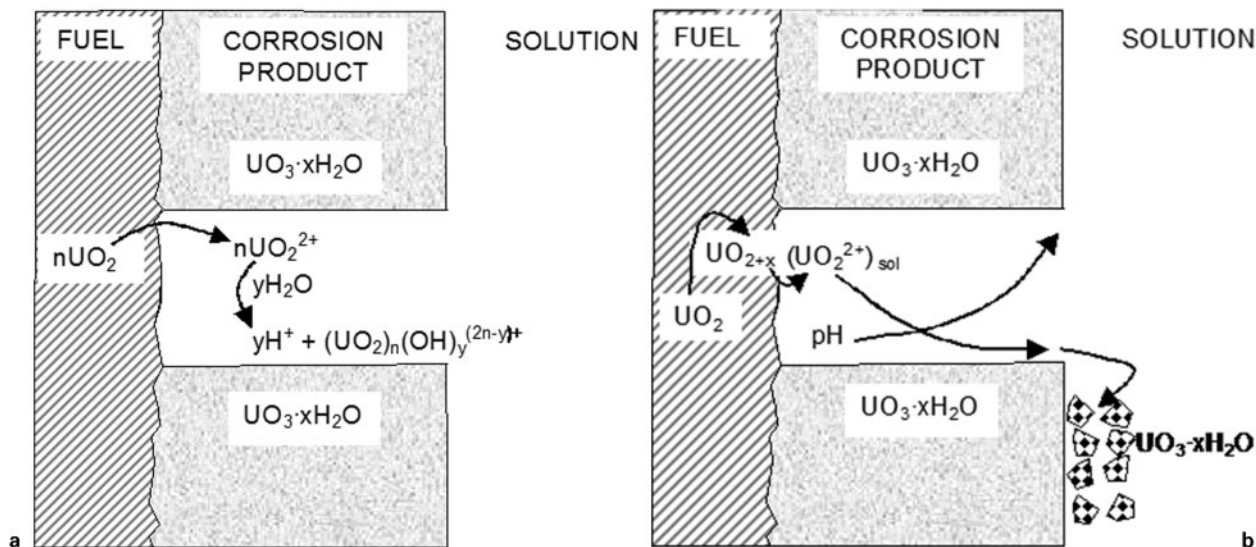
a hydrolysis of dissolved $U^{VI}O_2^{2+}$ produces low pH at corroding surface; *b* this leads to pH gradient and corresponding inverted solubility gradient (indicated by increasing and decreasing arrows, respectively) within pore

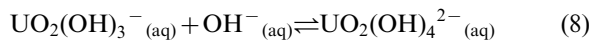**1 Schematic illustrations of influence of corrosion product deposit on local chemistry at corroding fuel surface**
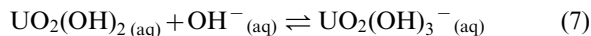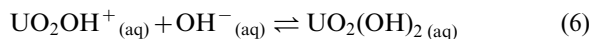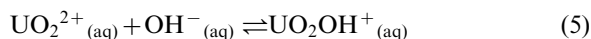
of the $U^{VI}O_2^{2+}$ dissolution product, as shown in Fig. 2. The base of the pore is the reactive fuel surface, while the mouth is open-ended, and the point at which U^{VI} species reach the surrounding groundwater solution. The walls of the pore are assumed to be non-reactive. In Fig. 2, U^{VI} species escaping the pore are assumed to be transported away from the mouth. A similar constant concentration condition could be achieved at this location if these species are immediately precipitated (Fig. 1*b*).

At steady-state, the mass balance within a cylindrical pore is governed by diffusion and chemical reactions

$$D_i \left[\frac{\partial^2 c_i(r,z)}{\partial r^2} + \frac{1}{r}\frac{\partial c_i(r,z)}{\partial r} + \frac{\partial^2 c_i(r,z)}{\partial z^2} \right] = -\sum_k R_i^m \quad (4)$$

where r and z are the coordinates in a radial direction and along the length of the pore, respectively, $C_i(r,z)$ and D_i are the concentration and the diffusion coefficient of species i, respectively, and R_i^m is the reaction rate of species i in reaction m. If i is a product in the reaction m, $R_i^m > 0$; on the other hand, if i is a reactant, $R_i^m < 0$.

The influx of dissolved $U^{VI}O_2^{2+}$ at the base of the pore will initiate hydrolysis reactions which consume OH^- (create H^+ from H_2O) and occur in concert with the H_2O equilibrium reaction
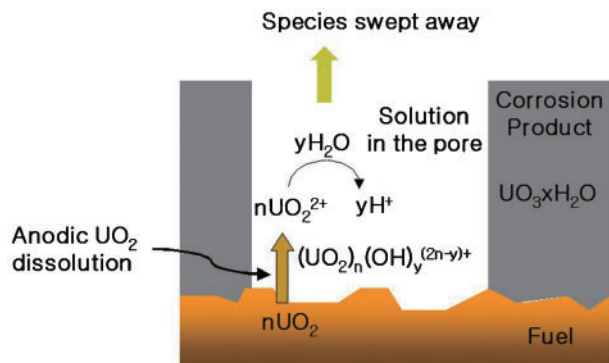

2 Illustration showing basic electrochemical and chemical processes considered in model

$$UO_2^{2+}{}_{(aq)} + OH^-{}_{(aq)} \rightleftharpoons UO_2OH^+{}_{(aq)} \quad (5)$$

$$UO_2OH^+{}_{(aq)} + OH^-{}_{(aq)} \rightleftharpoons UO_2(OH)_2{}_{(aq)} \quad (6)$$

$$UO_2(OH)_2{}_{(aq)} + OH^-{}_{(aq)} \rightleftharpoons UO_2(OH)_3^-{}_{(aq)} \quad (7)$$

$$UO_2(OH)_3^-{}_{(aq)} + OH^-{}_{(aq)} \rightleftharpoons UO_2(OH)_4^{2-}{}_{(aq)} \quad (8)$$

$$H_2O \rightleftharpoons H^+{}_{(aq)} + OH^-{}_{(aq)} \quad (9)$$

For reaction (9), $k_9 = 2\cdot518 \times 10^{-5}\ s^{-1}$ and $k_{-9} = 1\cdot4 \times 10^{11}\ L\ mol^{-1}\ s^{-1}$ were used for the forward and reverse rate constants, respectively.[12] For reactions (5)−(8), the equilibrium constants[13] were $K_5 = 6\cdot31 \times 10^8\ L\ mol^{-1}$, $K_6 = 7\cdot59 \times 10^8\ L\ mol^{-1}$, $K_7 = 1\cdot23 \times 10^5\ L\ mol^{-1}$, $K_8 = 1\cdot514\ L\ mol^{-1}$, and since the rate constants are unknown, the forward rate constants (k_f) were assumed to be $10^9\ L\ mol^{-1}\ s^{-1}$, and reverse rate constants calculated accordingly. The use of large k_f values makes hydrolysis relatively rapid, thus, enabling the calculation of the largest possible pH change.

The establishment of equilibrium conditions within the pore is also dependent on the diffusion rates of the U^{VI} species through the pore volume. Values of $10^{-6}\ cm^2\ s^{-1}$ were assumed for the diffusion coefficients for all species. This value is reasonable since the uranyl ion ($U^{VI}O_2^{2+}$) has a diffusion coefficient of 3–$6 \times 10^{-6}\ cm^2\ s^{-1}$,[14] and values of this magnitude are normal for relatively large ionic species.[15]

For the anodic dissolution of $U^{IV}O_2$, a relationship between applied potential and current has been defined.[4,16] This relationship has the Tafel form, indicating that the mechanism does not change with potential and that the relationship can be extrapolated to predict rates outside the range of the measurements. The flux condition at the base of the pore is thus defined by equation (10)

$$J_{UO_2^{2+}}(z=0) = \frac{10^{-6}\gamma}{nFA_0}\exp(-4\cdot4 + 16E) \quad (10)$$

where E is the potential [V(SCE)], $n(=2)$ is the number of electrons involved in the charge transfer reaction, F is

Faraday's constant, and A_0 is the electrode area (m^2). In the model the potential used in equation (10) to calculate the flux is equivalent to the corrosion potential enforced by the redox conditions inside the failed container, and is effectively determined by the α-radiation dose rate.

This flux-potential relationship assumes anodic dissolution is uniform across the U^{IV}O$_2$ surface. However, experiments at very low nominal current densities (1 to 300 nA cm^{-2}),[17] i.e. at currents more closely approaching those anticipated under disposal conditions (<0·1 nA cm^{-2}),[10] show dissolution is highly localised, the active area being considerably less than the geometric area. Since dissolution was confined to a relatively small fraction of the generally deposit-covered surface, an attenuation factor (γ) was introduced to account for the fact that the local current density will be considerably higher.

For this modelling approach to be representative of the dissolution process, the cathodic reaction (3) must occur external to the pore so that the alkalinity generated (reaction (3)) will not neutralise the acidity produced within the pore. A number of features of the fuel could maintain this separation of anodes and cathodes. The spent fuel matrix will be conducting due to rare-earth doping induced by the in-reactor fission process.[4,18] This feature, combined with the roughness of the fuel surface, could lead to anodic dissolution in deep locations supported by the cathodic reaction on more exposed areas of the surface. Additionally, noble metal particles within the conductive matrix could act as catalytic cathodes galvanically-coupled to remote anodic sites.[18,19]

An additional feature of the model, related to the movement of U species, is the ability of dissolved U^{VI} to escape to the bulk groundwater on reaching the pore mouth. This can be described by equation (11)

$$\hat{n} \cdot D_i \nabla C_i (z = d) = \alpha_i (C_{bi} - C_i) \tag{11}$$

where d is the pore depth, and α_i and C_{bi} are the mass transport coefficient and bulk concentration of species i, respectively. The values of α_i are assumed sufficiently large that species reaching the pore mouth would escape to the bulk solution, thereby maintaining a constant concentration at this location.

Simulation results and discussion

Numerical solutions were developed using COMSOL Multiphysics (COMSOL Inc.), a commercial simulation package based on the finite element method. The model was simulated using the diffusion mode in the chemical engineering module, COMSOL Multiphysics version 3.5. The default values of the simulation parameters are listed in Table 1. When used, different values are specified in the text.

pH distribution within the pore

Figure 3 shows the pH profile along the central line of a pore. The inset displays the two-dimensional pH distribution within the pore. As expected the pH varies with depth in the pore, but is independent of radial dimension. Consequently, it is only necessary to define pore depth (the diffusion path length). Since the concentration of U^{VI}O$_2^{2+}$ is greatest at the fuel surface at the pore base, the extent of hydrolysis is greatest and, therefore, the pH lowest at the base of the pore. This pH value is used in subsequent calculations.

Effect of flux attenuation (active dissolution area)

The calculated pH at the base of a pore is shown as a function of the attenuation factor for different E values (Fig. 4). Experimental data show that U^{IV}O$_2$ dissolution leading to local acidification can occur at applied potentials >250 mV.[7] Based on this observation we have chosen a flux attenuation factor of 10^3, which generates a slight pH depression at 100 mV, and a very significant one at 300 mV (Fig. 4). This flux attenuation value (γ=10^3) was adopted as the default value and is equivalent to a 0·1% surface activity.

Effect of pore depth and potential

Figure 5a and b shows the calculated pH as a function of pore depth and potential, respectively. These calculations show that significant acidification only occurs for a combination of high positive potentials and deep pores. The increase in potential increases the anodic dissolution rate of the fuel and, hence, the U^{VI}O$_2^{2+}$ flux at the fuel surface, and an increase in depth of the pore increases the diffusion path length. Both of these effects increase the local concentrations of U^{VI} species within the pore, and shift the equilibrium of reactions (5)–(8) to the right, leading to a pH decrease. A suppression of pH to a value <5 is achievable for highly oxidising conditions (E>250 mV), which is consistent with experimental data.[7] For the low potential of −250 mV, a suppression

Table 1 Default values of simulation parameters

Parameter	Symbol	Value	Unit
Pore depth	d	12	μm
Pore radius	r_0	2	μm
Diffusion coefficients for all U species	D_U	$1·0 \times 10^{-10}$	m^2 s^{-1}
Diffusion coefficient for H$^+$	D_H	$9·31 \times 10^{-9}$	m^2 s^{-1}
Diffusion coefficient for OH$^-$	D_{OH}	$5·30 \times 10^{-9}$	m^2 s^{-1}
Forward rate constants for reactions (5)–(8)	k_f	1×10^6	m^3 mol^{-1} s^{-1}
Forward rate constant for reaction (9)	k_9	$2·518 \times 10^{-5}$	s^{-1}
Backward rate constant for reaction (9)	k_{-9}	$1·4 \times 10^8$	m^3 mol^{-1} s^{-1}
Attenuation factor for UO$_2$ flux at pore bottom	γ	1000	
Value of pH in bulk solution	(pH)$_b$	9·5	
Bulk concentrations of all U species	C_b	0	mol m^{-3}
Transfer coefficients for all species at pore opening	α	1	
Potential on UO$_2$ surface*	E	200	mV

*All potentials are reported with the reference to a saturated calomel electrode (SCE).
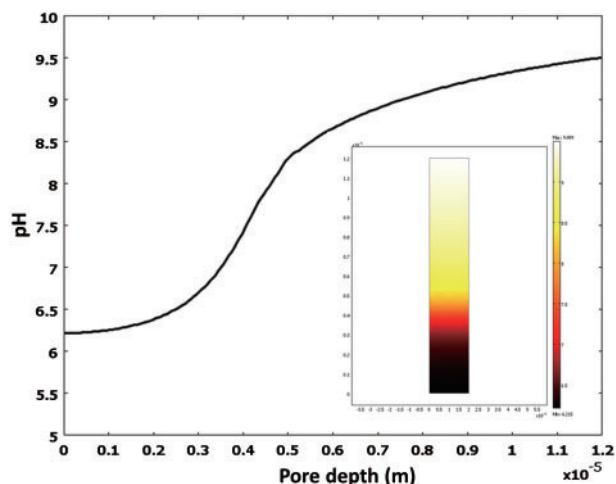
3 pH profile along centre line of pore using default simulation conditions. Inset shows two-dimensional pH distribution

of the pH to a value <5 is not achievable for any pore depth up to 1 cm (Fig. 5a).

Some differences in the shapes of the plots are observed in Fig. 5b. At very positive potentials the pH reaches a plateau less readily for the deeper pores. For a chemical system such as this one, the achievement of a plateau would be analogous to an acid-base equilibrium, the overall plot being similar to the titration of a weak base with an acid (i.e. pH vs volume of acid compared to pH vs potential). The lack of a plateau at positive potentials for the deeper pores suggests a mixed diffusional–chemical control of the pH at the fuel surface as a consequence of the shallower concentration gradient along the longer diffusion path from the fuel surface to the bulk of solution.

Conditions for accelerated UO$_2$ dissolution under disposal conditions

There is experimental evidence[20] to show the UO$_2$ dissolution rate increases significantly for pH<5. Since the pore pH depends on the flux attenuation, pore depth, and potential, it is useful to define the conditions
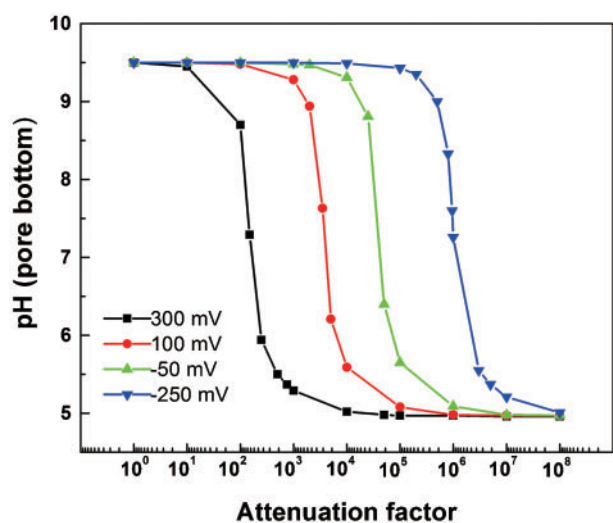
4 Simulated pH at base of pore as a function of flux attenuation factor (γ)

under which fuel dissolution could be accelerated. In Fig. 6, the range of flux attenuation/pore depth values above each line are those for which the pH at the bottom of the pore can be suppressed to values <5; i.e. a region in which the fuel dissolution rate can begin to accelerate as a consequence of local acidification. For example, at $E=300$ mV and $\gamma=1000$, pH<5 would be achievable in a pore deeper than 18 μm, while at $E=-50$ mV (with the same γ), the pore must be 80 times deeper.

These calculated values can be compared to the values predicted for corrosion potentials and the thickness of corrosion product deposits inside a failed waste container.[10] According to this conservative model,[10] providing the container fails immediately on emplacement in the repository, the corrosion potential will range from an initial value of -50 mV(SCE) when radiolytic oxidising conditions prevail to about -250 mV after 10^6 years when anoxic conditions would exist. Comparison to Fig. 6 shows that very thick corrosion product deposits (>1 mm) would have to form rapidly on first exposure of the fuel to the groundwater if the possibility of acidification was to occur. Such a rapid conversion of the fuel (U^{IV}O$_2$→U^{VI}O$_3$.yH$_2$O) is not possible at the α-radiation dose rates available.[10] Even though this model[10] does not include many of the features expected to inhibit fuel corrosion (such as H$_2$ produced within a failed container[17]) calculations indicate that the generation of such thick corrosion product layers would require tens of thousands of years.

Summary and conclusions

The corrosion of spent nuclear fuel leading to radionuclide release within a failed waste container in a Canadian repository would be driven by oxidants produced by the radiolysis of water. Since the fuel matrix is conductive with a rough surface and contains noble metal particles, the spatial separation of cathodes (e.g. noble metal particles) and anodes (pores in corrosion product deposits/fractures in the fuel pellets) may be possible, introducing the possibility of the hydrolysis of dissolved UO$_2^{2+}$ to produce acidification at anodic sites. This acidity could accelerate dissolution at these locations.

The development of acidity within pores in corrosion products on fuel has been modelled. The model couples diffusion, chemical reactions and the interfacial electrochemical dissolution process, and was solved numerically. The simulations show the build-up of acidity is possible within flaws and pores, and the extent to which the pH is depressed is influenced by the dimensions of the defect and the redox conditions (expressed as a potential). The simulations also show that a significant depression can only be achieved if the fuel dissolution rate is attenuated to reflect a highly localised corrosion process.
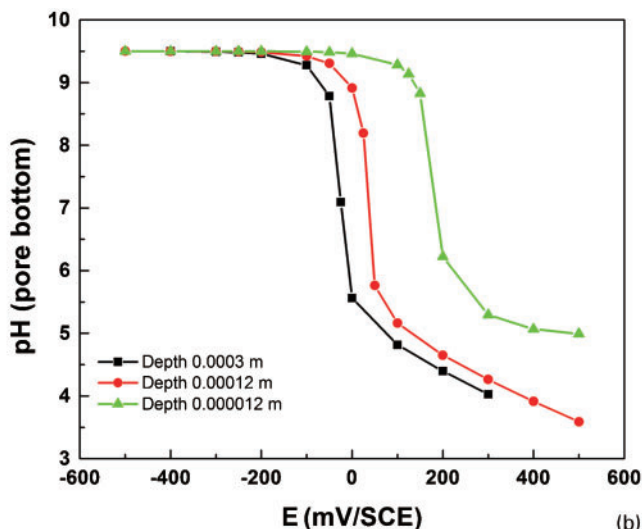
A comparison to the redox conditions anticipated in a failed waste container indicates that the conditions required for the development of acidity that fuel dissolution could be accelerated will not occur.
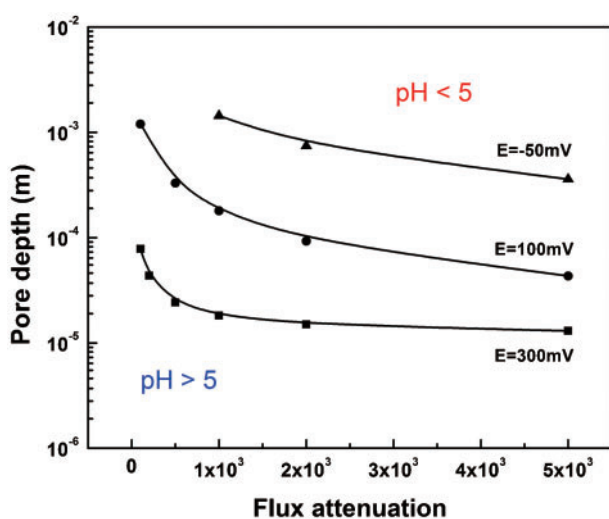
Acknowledgements
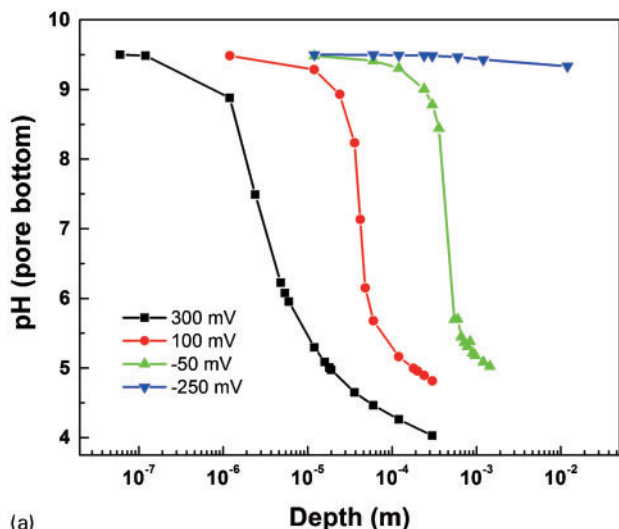
5 Simulated pH at base of pore as a function of *a* pore depth and *b* potential

6 Conditions when pH<5 at bottom of pore could be achieved

References

 1. Nuclear Waste Management Organization: 'Choosing a way forward: the future management of Canada's used nuclear fuel', NWMO Report, 2005.
 2. F. King and M. Kolar: 'The copper container corrosion model used in AECL's second case study', Ontario Power Generation report: 06819-REP-01200-10041-R00, 2000.
 3. D. W. Shoesmith, J. J. Noel, Z. Qin, C. T. Lee, J. S. Goldik, B. G. Santos and M. E. Broczkowski. 'Corrosion of nuclear fuel (UO$_2$) inside a failed nuclear waste container', Ontario Power Generation report: 06819-REP-01200-10145-R00, 2005.
 4. D. W. Shoesmith: 'Fuel corrosion processes under waste disposal conditions', *J. Nucl. Mater.*, 2000, **282**, 1–31.
 5. D. W. Shoesmith: 'Used fuel and uranium dioxide dissolution studies – A review', NWMO Report No. TR-2007-03, 2007.
 6. I. Grenthe, J. Fuger, R. J. M. Konings, R. J. Lemire, A. B. Muller, C. Nguyen-Trong and H. Wanner: in 'Chemical thermodynamics', (ed. H. Wanner and I. Forest), Vol. 1; 1992, Amsterdam, North Holland.
 7. B. G. Santos, J. J. Noel and D. W. Shoesmith: 'The influence of potential on the anodic dissolution of SIMFUEL (UO2)', *Electrochim. Acta*, 2006, **51**, 4157–4166.
 8. D. W. Shoesmith, S. Sunder, M. G. Bailey and N. H. Miller: 'Oxidation and dissolution (corrosion) of used fuel electrodes in aqueous perchlorate and carbonate solutions', *J. Nucl. Mater.*, 1996, **227**, 287–299.
 9. J. C. Wren, D. W. Shoesmith and S. Sunder: 'Corrosion behavior of uranium dioxide in alpha radiolytically decomposed water', *J. Electrochem. Soc.*, 2005, **152**, B470–B481.
10. D. W. Shoesmith, M. Kolar and F. King: 'A mixed-potential model to predict fuel (uranium dioxide) corrosion within a failed nuclear waste container', *Corrosion*, 2003, **59**, 802–816.
11. L. Wu, Y. Beauregard, Z. Qin, S. Rohani and D. W. Shoesmith: 'A model for the influence of steel corrosion products on nuclear fuel corrosion under permanent Disposal Conditions', *Corros. Sci.*, 2012, **61**, 83–91.
12. P. W. Atkinson: 'Physical chemistry', 2nd edn, 1072; 1982, New York, W.H. Freeman and Company.
13. D. W. Shoesmith, S. Sunder and W. H. Hocking: in 'Electrochemistry of novel materials', (ed. J. Lipkowski and P. N. Ross), Chapter 6; 1994, New York, VCH.
14. J.-P. Simonin, I. Billard, H. Hendrawan, O. Bernard, K. Lützenkirchen and L. Sémon: 'Study of kinetic electrolyte effects on a fast reaction in solution: the quenching of fluorescence of uranyl ion up to high electrolyte concentration', *Phys. Chem. Chem. Phys.*, 2003, **5**, 520–527.
15. R. G. Robinson and R. H. Stokes: 'Electrolyte solutions'; 1960, London, Longman.
16. S. Sunder, L. K. Strandlund and D. W. Shoesmith: 'Anodic oxidation and dissolution of CANDU fuel (UO2) in slightly alkaline sodium perchlorate solutions', *Electrochim. Acta*, 1998, **43**, 2359–2372.
17. D. Ofori, P. G. Keech, J. J. Noel and D. W. Shoesmith: 'The influence of deposited films on the anodic dissolution of uranium dioxide', *J. Nucl. Mater.*, 2010, **400**, 84–93.
18. H. He, M. Broczkowski, K. O'Neil, D. Ofori, O. Semenikhin and D. W. Shoesmith, 'Corrosion of nuclear fuel inside a failed nuclear waste container: a review of research conducted under the industrial research chair agreement between NSERC, NWMO and Western university (January 2005 to December 2010)', NWMO-TR-2011-20, February 2012.
19. M. E. Broczkowski, P. G. Keech, J. J. Noel and D. W. Shoesmith: 'Corrosion of uranium dioxide containing simulated fission products in dilute hydrogen peroxide and dissolved hydrogen', *J. Electrochem. Soc.*, 2010, **157**, C275–C281.
20. M. E. Torrero, E. Baraj, J. de Pablo, J. Gimenez and I. Casas, 'Kinetics of corrosion and dissolution of uranium dioxide as a function of pH', *Int. J. Chem. Kinet.*, 1997, **29**, 261–267.